

Anomalous localization in spin-chain with tilted interactions

Arindam Mallick^{1,*} and Jakub Zakrzewski^{1,2,†}

¹*Instytut Fizyki Teoretycznej, Uniwersytet Jagielloński, Lojasiewicza 11, 30-348 Kraków, Poland*

²*Mark Kac Complex Systems Research Center, Uniwersytet Jagielloński, Kraków, Poland*

(Dated: January 26, 2024)

The localization properties of a disorder-free spin chain with inhomogeneous interactions are studied. In particular, we consider interaction strength growing linearly along the chain for systems with different interaction ranges. Using exact diagonalization we find the participation ratio of all eigenstates which allows us to quantify the localization volume in the Hilbert space. Surprisingly the localization volume changes nonmonotonically with the interaction range. The model for the infinite interaction range resembles the Schwinger model of lattice gauge theory in staggered formalism. The model studied may be implemented in state-of-the-art cold atomic devices and could reveal hidden features in disorder-free confinement phenomena.

I. INTRODUCTION

Localization properties or in general non-ergodicity at the quantum many-particle level have been attracting physicists for more than half of a century [1], as it breaks the conventional understanding of thermalization in classical physics. One major branch deals with the random [1–4] or quasi-periodic disorder [5–8] induced localization. Recently another branch—localization without disorder—is catching a lot of attention. The latter happens in the presence of energy constraints e.g. linear tilt (DC field) or harmonic traps [9–15], gauge field induced confinement [16–22]; in the presence of other species of particles which effectively induce random environment [23, 24]; in presence of flatbands [25]; etc. The study of long-range e.g. dipolar interaction effects on such models has also a rich history [26–33] with recent progress being related to the experimental progress in cooling and trapping of dipolar matter [34–36].

In this article, we introduce a one-dimensional (1D) spin chain model in which the interaction strength is inhomogeneous and, in particular, increases with the distance along the lattice. While typically the interaction strength decays as a power law or exponentially with the distance [31, 37] we consider the case where it grows linearly, not only with respect to the relative distance but also with the explicit location of spins. In that way, it also differs from the 1D Coulomb model in the continuum where interaction strength grows with the relative distance between charge densities only [38]. By numerical full diagonalization using the Quspin python library [39, 40] we study the localization volume, i.e. the participation ratio (PR) in the Hilbert space spanned by the eigenstates of spin-half σ^z operator, as a function of the range of interactions and their strength. Therefore our study captures not only the near zero temperature case but also all temperature cases. The nearest neighbor case of our model is similar to the recently studied Hamilto-

nian in Ref. [41].

Stronger interactions turn the hopping or spin-flip less probable, and Hamiltonian eigenstates appear more similar to the spin-aligned states or the eigenstates of σ^z operators. The alignment becomes more robust and locally conserved as we move from left to right of the chain with linearly growing interaction strength. This phenomenon is similar to the Hilbert space fragmentation leading to the presence of conserved local operators [42–44]. Therefore a stronger interaction reduces the Hilbert space occupation, the localization volume—as observed in our work and as reported recently [41]. This happens irrespective of the range of interactions. On the other hand, the longer the range of interactions is, induces longer the correlations and one expects to see always an increase in the localization volume. But, surprisingly, we observe that the localization volume reduces upon increasing the range and after an intermediate range, it again starts to grow. Such a nonmonotonic behavior was not reported before in any clean (disorder-free) lattice model. We explain this phenomenon by moving from a spin picture to the particle occupation picture. We show that there is an interplay between the fragmentation induced by two-body interactions and an effective tilt potential induced by longer-ranged interaction.

The paper is organized as follows. We introduce our model and measures studied in Section II. Section III is dedicated to our numerical full diagonalizations, the extraction of relevant results for clean systems with various ranges of interactions, and an explanation of the results. The section IV is dedicated to the effect of quasi-periodic additive disorder on clean systems. We conclude in section V. Appendix A describes the connection of our clean Hamiltonian with the lattice gauge theory.

II. MODEL

Here we define the spin-half Hamiltonian on a 1D finite chain with various ranges of tilted ZZ interaction

* arindam.mallick@uj.edu.pl

† jakub.zakrzewski@uj.edu.pl

$$\mathcal{H}_{\mathcal{R}} = -t \sum_{n=0}^{L-2} (\sigma_n^+ \sigma_{n+1}^- + \sigma_n^- \sigma_{n+1}^+) + U \sum_{l=1}^{\mathcal{R}} \sum_{n=0}^{L-(l+1)} (n+l) \sigma_n^z \sigma_{n+l}^z \quad (1)$$

where the range \mathcal{R} can take any value from the integer set $\{1, 2, 3, \dots, L-2, L-1\}$. At $\mathcal{R} = L-1$ our model is similar to the lattice Schwinger model of staggered spinless fermions after integrating out the electromagnetic gauge degrees of freedom—see Appendix A for details. We use the notation $\sigma_n^+ = \begin{pmatrix} 0 & 1 \\ 0 & 0 \end{pmatrix} = (\sigma_n^-)^\dagger$, $\sigma_n^z = \frac{1}{2} \begin{pmatrix} 1 & 0 \\ 0 & -1 \end{pmatrix}$ for all lattice site n . U is the interaction strength parameter while t is the hopping amplitude put to unity from now on.

Note that the interaction strength in the model (1) depends not only on the relative distance $l = (n+l) - n$ between spins but also depends on the spins' location. The Hamiltonian possesses two obvious symmetries: It commutes with and hence dynamically conserves associated eigenvalues of (i) total magnetization operator $\sum_{n=0}^{L-1} \sigma_n^z$ and (ii) product of all spin-flip operators $\prod_{n=0}^{L-1} \sigma_n^x$. We consider an even number of lattice sites and only zero magnetization sector $\sum_{n=0}^{L-1} \sigma_n^z = 0$ such that the total number of spin-up = the total number of spin-down. This corresponds to the maximum Hilbert space dimension compared to other magnetization sectors, and it is similar to the half-filled spinless fermions. The zero magnetization sector can be divided into two mutually orthogonal vector spaces concerning the \mathbb{Z}_2 symmetry induced by the product of spin-flip operators: they consist of “linear superposition” of $\prod_{n=0}^{L-1} \sigma_n^z$ eigenstates which are either symmetric having eigenvalue +1 or antisymmetric having eigenvalue -1 under the action of $\prod_{n=0}^{L-1} \sigma_n^x$. The total number of basis states $|s_j\rangle$ in the symmetric sector is equal to that in the antisymmetric sector. Therefore the Hilbert space dimension of one of the sectors is

$$\mathcal{D} = \frac{L!}{2[(L/2)!]^2}. \quad (2)$$

We consider the symmetric sector only while analyzing the clean system. For the system size $L = 18$ and 16 the $\mathcal{D} = 24310$ and 6435 , respectively. We numerically diagonalize the full Hamiltonian in this sector for different \mathcal{R} , U , and for different chain lengths L with open boundary conditions. We concentrate mainly on the second participation entropy [45] for the eigenvector $|\psi_E\rangle$ at each eigen-energy E

$$\mathcal{S}(E) = -\ln \left(\sum_{j=1}^{\mathcal{D}} | \langle s_j | \psi_E \rangle |^4 \right), \quad (3)$$

calculated in the $\{|s_j\rangle\}$ basis defined above. For mutually unbiased basis $\{|s_j\rangle\}$ and the set of eigenvectors

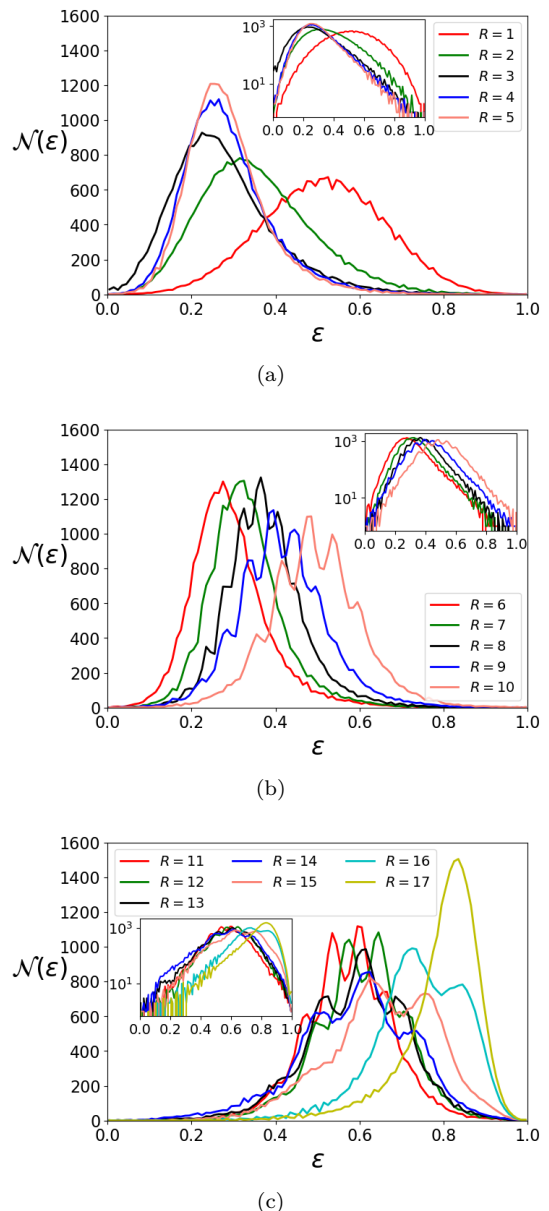


FIG. 1. Envelope plots of the histograms of the number of states $\mathcal{N}(\varepsilon)$ as a function of ε [Eq. (4)] for different \mathcal{R} as indicated in the panels, while $U = 1.2$ and $L = 18$ for all subplots. 100 bins are used during histogram analysis for all cases. The insets are the same plots as in the main panels but on a log-linear scale.

[46] one may expect that for a fully ergodic system with equal probability amplitude at $|s_j\rangle$ for all j , $\mathcal{S}(E) = \ln \mathcal{D}$. While for a nonergodic system with singly occupied $|s_j\rangle$ state $\mathcal{S}(E) = 0$. This implies $\mathcal{S}(E)/\ln \mathcal{D} \in [0, 1]$. Therefore the $\mathcal{S}(E)$ captures the localization volume in symmetric spin-space.

III. NUMERICAL RESULTS

To take care of the energy dependence of our problem we follow the standard by now procedure [47] and scale the energy eigenvalues, E , as

$$\varepsilon = (E - E_{\min}) / (E_{\max} - E_{\min}) \in [0, 1]. \quad (4)$$

Figure 1 shows the number of states at different energies with the variation of range for $L = 18$ and $U = 1.2$. Two observations follow. Firstly, with the increase of the range of interactions, the maximum of the density shifts first to smaller ε values then it comes back near to the center again and, for still larger \mathcal{R} moves towards right $\varepsilon = 1$. Secondly, for intermediate \mathcal{R} distinct peaks appear in the \mathcal{N} profile which is a clear sign of a Hilbert space fragmentation-like effect. For longer \mathcal{R} the peak heights as well as the number of peaks in a distribution reduce with an increase of \mathcal{R} .

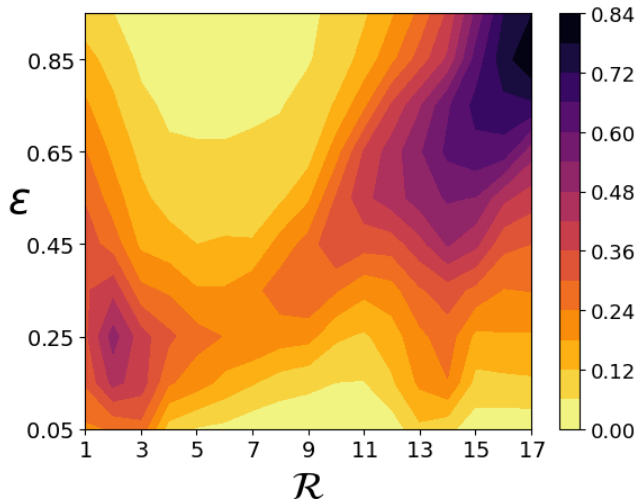


FIG. 2. Participation entropy $\mathcal{S}/\ln \mathcal{D}$ averaged over the energies within each bin in energy histogram [Fig. 1], as a function of scaled energy and range. $U = 1.2$, $L = 18$.

To analyze the energy-resolved participation entropy we consider 10 bins in ε . Note, parenthetically, that we consider a disorder-free system so no disorder average is possible. That explains some of the fluctuations observed in different figures. We average the entropy over all eigenvalues within each bin. Figure 2 depicts the result which shows maximum \mathcal{S} near the maximum peak in Fig. 1 for any \mathcal{R} . Interestingly for almost all energies at some intermediate values of \mathcal{R} the localization volume in spin Hilbert space i.e. the the participation entropy is lower compared to the shorter and longer ranges.

Next, we focus on the peak density of states by considering the following set of eigenvalues

$$\mathcal{Z} = \{\varepsilon : \ln[\mathcal{N}(\varepsilon)] \geq 0.9 \max\{\ln[\mathcal{N}(\varepsilon)]\}\}. \quad (5)$$

The natural logarithm is taken to smoothen the distributions—compare the insets and main plots in

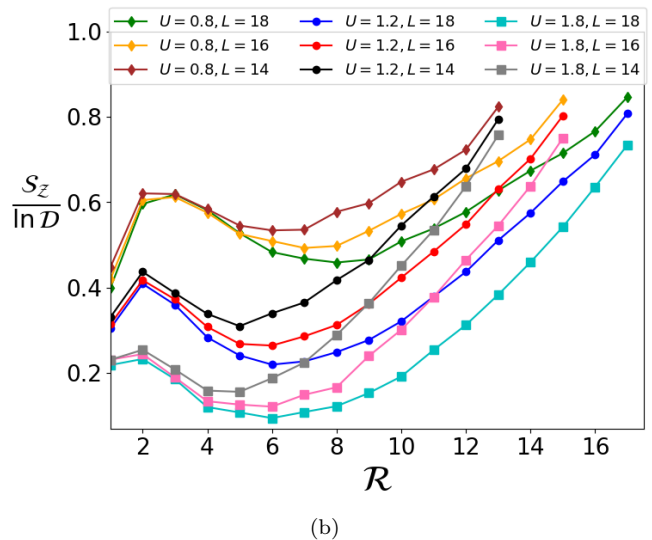
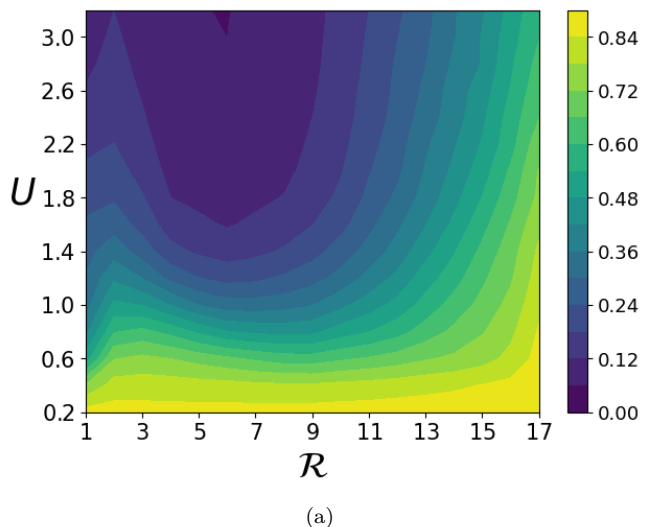


FIG. 3. (a) Participation entropy $\mathcal{S}_{\mathcal{Z}}/\ln \mathcal{D}$, i.e. $\mathcal{S}/\ln \mathcal{D}$ averaged over the set \mathcal{Z} [Eq. (5)], as a function of U and \mathcal{R} . $L = 18$. (b) $\mathcal{S}_{\mathcal{Z}}/\ln \mathcal{D}$ for different system sizes $L = 14$ ($\mathcal{D} = 1716$), 16 ($\mathcal{D} = 6435$), 18 ($\mathcal{D} = 24310$), and different U .

Fig. 1 for details. The participation entropy averaged over all eigenstates that belong to \mathcal{Z} , labeled as $\mathcal{S}_{\mathcal{Z}}$ is plotted as a function of U and \mathcal{R} in Fig. 3. The nonmonotonic or anomalous behavior of the localization volume as a function of range for almost all U and all system sizes is visible. The intermediate range $\mathcal{R} = \mathcal{R}_c$ for which the minimum occurs shifts to larger values with an increase of system size L at a fixed U . On the other hand for a fixed L increase of U shifts the \mathcal{R}_c to smaller values. Larger system size L , at a fixed range \mathcal{R} and fixed U leads to smaller $\mathcal{S}_{\mathcal{Z}}$ indicating that the behavior observed is not due to the small system size.

A. Localization transition analysis

We now compare the participation entropies for different system sizes in units of $\ln \mathcal{D}$ to extract possible system size independent crossing points similar to the analysis done in [45].

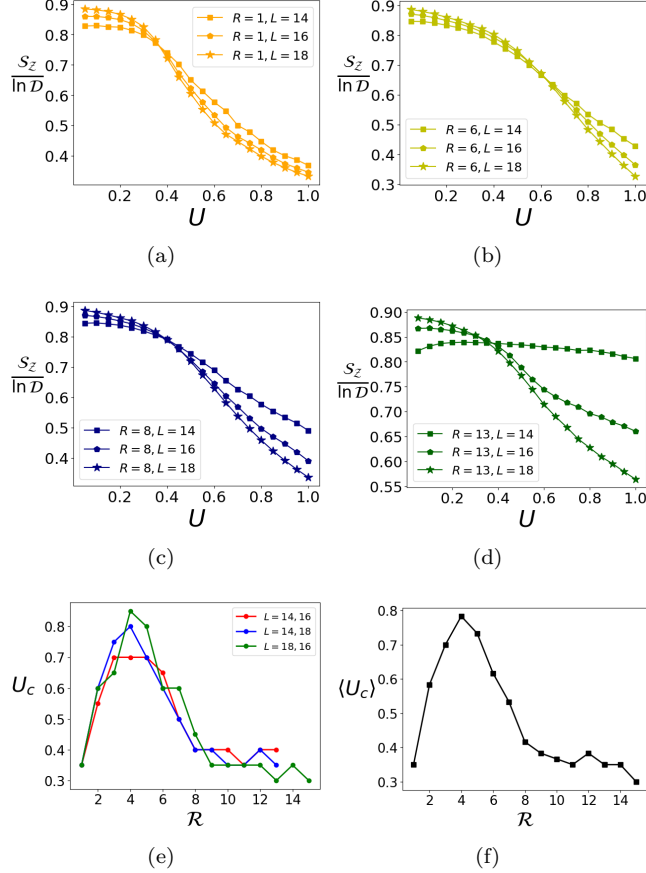


FIG. 4. Plots (a)-(d): $\mathcal{S}_{\mathcal{Z}}/\ln \mathcal{D}$ as a function of interaction parameter $U \geq 0.05$ for various L and \mathcal{R} . The crossing point at each subplot is associated with the ergodic to nonergodic transitions. (e) The transition interaction parameter U_c as a function of range extracted from different L combinations. (f) Averaged U_c over all combinations in subfigure (e).

We plot $\mathcal{S}_{\mathcal{Z}}/\ln \mathcal{D}$ as a function of interaction parameter U for different ranges and system sizes in Fig. 4(a)-(d): only four \mathcal{R} cases are shown for convenience. The crossing point for different L appears approximately at the same point $U = U_c$ for any fixed \mathcal{R} . A closer inspection reveals that it also shows a nonmonotonic behavior with \mathcal{R} . For small \mathcal{R} the crossing point happens for smaller values of U , it shifts to larger U at intermediate ranges, and for longer ranges it again moves to smaller U values. The crossing points are associated with the ergodic to nonergodic transitions [45]. We conjecture that the crossing point approaches $U \rightarrow 0$ when $\mathcal{R} \rightarrow \infty$ which is possible at $L \rightarrow \infty$ which signifies the appearance of nonergodic behavior for arbitrarily small U in massless

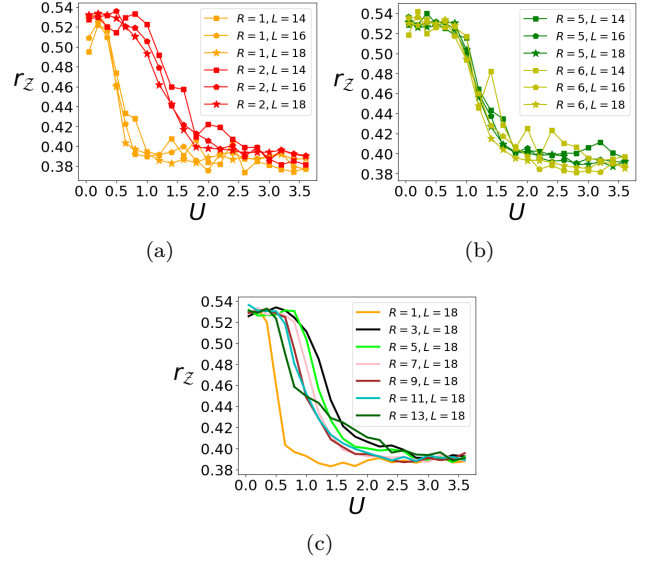


FIG. 5. (a)-(c) Spectral gap ratio r averaged over the set \mathcal{Z} as a function of U for various L and \mathcal{R} . 100 bins are used for all cases.

clean Schwinger like models. To calculate the value of U_c for each \mathcal{R} we consider three crossing points of three pairs of curves: (i) $\mathcal{S}_{\mathcal{Z}}/\ln \mathcal{D}$ for $L = 14$ and $L = 16$ when $\mathcal{R} \leq 13$, (ii) $\mathcal{S}_{\mathcal{Z}}/\ln \mathcal{D}$ for $L = 14$ and $L = 18$ when $\mathcal{R} \leq 13$, and (iii) $\mathcal{S}_{\mathcal{Z}}/\ln \mathcal{D}$ for $L = 16$ and $L = 18$ when $\mathcal{R} \leq 15$. Numerically the crossing point is defined as the data coordinate $(U, \mathcal{S}_{\mathcal{Z}}/\ln \mathcal{D})$ where the absolute value of the difference of $\mathcal{S}_{\mathcal{Z}}/\ln \mathcal{D}$ for two different L is minimum. The result is depicted at Figs. 4(e)-(f) which clearly captures a nonmonotonic behavior with \mathcal{R} . For stronger U we have shown the participation entropy plots in the appendix B.

The anomalous effect is also visible in the spectral gap ratio

$$r_{\alpha} = \frac{\min\{\varepsilon_{\alpha+1} - \varepsilon_{\alpha}, \varepsilon_{\alpha} - \varepsilon_{\alpha-1}\}}{\max\{\varepsilon_{\alpha+1} - \varepsilon_{\alpha}, \varepsilon_{\alpha} - \varepsilon_{\alpha-1}\}} \quad (6)$$

where α is the index of the sorted eigenvalues in ascending order. Figure 5 shows the spectral gap ratio r averaged over all α for which $\varepsilon_{\alpha}, \varepsilon_{\alpha\pm 1}$ belong to the set \mathcal{Z} as a function of U for different ranges. We labeled it as $r_{\mathcal{Z}}$. The crossing points U_c in Figs. 4(e)-(f) correspond to the $r_{\mathcal{Z}}$ values corresponding to the entrance of the system from the ergodic regime to the nonergodic regime.

B. Discussion

To explain the anomalous localization behavior, it is convenient to switch from the spin language to an equivalent spinless fermions description. We define the particle number operator at site n as $\hat{N}_n = \sigma_n^z + \frac{1}{2}$, relating the spin-up (spin-down) state to the presence (absence) of a particle. Only single occupancy at a lattice

site is possible. The σ_n^\pm operators are transferred into creation/annihilation operators for particles and the first line in (1) gives the standard kinetic energy term (describing hopping). The interactions part becomes

$$\begin{aligned} \mathcal{H}_{\text{in}} &= U \sum_{l=1}^{\mathcal{R}} \sum_{n=0}^{L-(l+1)} (n+l) \sigma_n^z \sigma_{n+l}^z \\ &= U \sum_{l=1}^{\mathcal{R}} \sum_{n=0}^{L-(l+1)} (n+l) \hat{N}_n \hat{N}_{n+l} \\ &\quad - \frac{U}{2} \sum_{l=1}^{\mathcal{R}} \sum_{n=0}^{L-(l+1)} (n+l) (\hat{N}_n + \hat{N}_{n+l}) \end{aligned} \quad (7)$$

where we neglected the additional constant interaction energy term. The first term above is the two-body interaction operator. The second line strongly resembles the tilted potential present in recent studies of disorder-free many-body localization [9–11, 15, 48]. We use the term “tilted potential” referring to the single particle potential term in the last line of Eq. (7) and “two-body interaction part” to discuss the first term in (7). The tilted interaction stands for the full ZZ-interactions term.

Two-body interaction part: The important fact about the two-body interacting term is that any particle at right position $(n+l)$ has the same energy of interaction with any particle at left site $(n+r) < (n+l)$ for various r (r can be negative or positive) while the relative distance between them is $(l-r)$. Therefore the absolute position of the left particle does not influence the two-body interaction term for a fixed position of the right particle at any relative distance. Thus all the “left” particles belonging to different pair configurations have the same interaction energy that may lead to resonance features. The interaction energy only changes if the location of the “right” particle changes. For an interaction range \mathcal{R} any site (except the sites $n = 0, 1, \dots, \mathcal{R} - 1$) possesses \mathcal{R} number of degenerate/resonating pairs. A particle at $n = 1$ possesses only one pair with $n = 0$, a particle at $n = 2$ possesses two such pairs with $n = 0$ and $n = 1$, etc. Such different sets of pairs corresponding to particles at different right locations $(n+l)$ fragment the whole accessible Hilbert space into disconnected domains. The number of possible pairs for a particle at fixed right position $(n+l)$ grows as \mathcal{R} grows. Therefore even if the two-body interaction causes Hilbert space fragmentation the growth of individual fragmented domains could cause an increase in localization volume. Moreover, there may exist some configurations of the particle distributions that correspond to the presence of extra particles in between the lattice sites that formed a pair. In that case, the extra particles will be connected with the particle forming the pair and among themselves by shorter range $< \mathcal{R}$ of interactions, and they change the energy of the configuration. Such configurations induce more fragmentation in the Hilbert space.

Tilted potential part: The tilted effective potential

part in the particle picture for a general \mathcal{R} reads

$$\begin{aligned} V_{\mathcal{R}} &= -\frac{U}{2} \sum_{l=1}^{\mathcal{R}} \sum_{n=0}^{L-(l+1)} (n+l) (\hat{N}_n + \hat{N}_{n+l}) \\ &= -\frac{U}{2} \sum_{l=1}^{\mathcal{R}} \left[\sum_{n=0}^{l-1} (n+l) \hat{N}_n + \sum_{n=L-l}^{L-1} n \hat{N}_n \right. \\ &\quad \left. + \sum_{n=l}^{L-(l+1)} (2n+l) \hat{N}_n \right] \\ &= -U \sum_{n=0}^{L-1} (\mathcal{R}n) \hat{N}_n + \frac{U}{2} \sum_{n=0}^{\mathcal{R}-1} n (\mathcal{R}-n) \hat{N}_n \\ &\quad + \frac{U}{4} \sum_{n=0}^{\mathcal{R}} [2nL + n(n-1)] \hat{N}_{L-\mathcal{R}+n-1}. \end{aligned} \quad (8)$$

For convenience we denote $V_{\mathcal{R}}/U$ as $\sum_{n=0}^{L-1} \mathcal{V}(n) \hat{N}_n$.

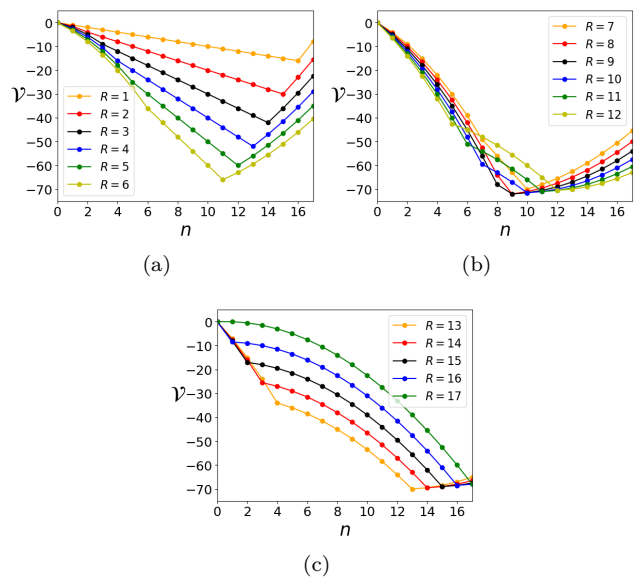


FIG. 6. The tilted potential [Eq. (8)] as a function of lattice site n . The plots are for various ranges in units of U for fixed system size $L = 18$.

In the last two lines of the above expression (8) while changing the double index sum to a single index sum we have omitted the extra additive term $= -(UL/4) \sum_{l=1}^{\mathcal{R}} l$ which comes from the total magnetization or particle number conservation: $\sum_{n=0}^{L-1} \hat{N}_n = L/2$ for even L . For detailed derivation see Appendix C.

Note, importantly, that, after representing the single-particle potential in terms of single index sums it contains both the linear and square terms in site number. That complicates its analysis. The presence of the linearly tilted potential may induce another type of fragmentation in Hilbert space due to an approximate conservation of the dipole moment as extensively discussed already [42, 43]. Such a clean situation almost occurs for $\mathcal{R} = 1$,

compare Fig. 6(a). However, the potential becomes quite different for a general \mathcal{R} forming first a triangular-like well with the minimum shifting close to the center of the lattice and changing its shape completely for longer ranges c.f. Fig. 6. The $V_{\mathcal{R}}$ effectively consists of three parts: the central region, and two sets associated with the sites near the two edges. Three different tilted parts become prominent for $\mathcal{R} \geq 9$. Instead of linear tilt, they resemble two concave curves (left and central) and one convex curve (right). For longer $\mathcal{R} \geq 13$ the central region grows and the potential resembles a single concave quadratic curve.

Simultaneous effect of two-body interaction and the tilted potential:

Consider small \mathcal{R} with a triangular well structure. The tilt of the potential is quite strong (for U of the order of unity) resulting locally in a very strong localization. It has been shown elsewhere [15, 48, 49] that the localization properties for sufficient tilt depend on the local effective “electric field” inducing the tilt. Thus increasing \mathcal{R} in this region should enhance localization leading to smaller U_c being needed for a nonergodic behavior. As depicted in Fig. 4(e) the situation is the opposite. Apparently, the effect of increased tilt is overcome by the increased range of interactions that mix the dynamics. The trend is reversed for $\mathcal{R} \geq 5$, the two-body interaction term becomes dominant and it induces Hilbert-space fragmentation lowering U_c . This qualitatively explains the nonmonotonic behavior of U_c as a function of \mathcal{R} in Fig. 4(e)-(f).

Hilbert space fragmentation divides the whole system into several disconnected parts, while correlations exist among states inside each fragmented part. An analysis of possible degenerate pairs suggests that the presence of a positive gradient part ($\partial V/\partial n > 0$) in tilted potential reduces the number of states inside each fragmented part and the total number of fragmented parts reduces. This is visible from the growing subpeak volumes in the number of state distributions in Fig. 1(b)-(c). This qualitatively explains the growing participation entropy $\mathcal{S}_{\mathcal{Z}}$ beyond $\mathcal{R} \geq 7$ with an increase of \mathcal{R} , e.g. Fig. 3 for a fixed U , even if the system is in the nonergodic regime.

IV. THE PRESENCE OF QUASI-PERIODIC DISORDER

To understand the anomalous localization behavior better and to check its robustness we add quasiperiodic disorder on the original clean Hamiltonian (1). The new Hamiltonian reads

$$\mathcal{H}_{\text{dis}} = \mathcal{H}_{\mathcal{R}} + \frac{W}{2} \sum_{n=0}^{L-1} \cos(2\pi\beta n + \pi\varphi) \sigma_n^z \quad (9)$$

where β is the golden ratio $= (\sqrt{5} + 1)/2$ and the site independent phase φ is a random number picked from a uniform distribution $\in [0, 1]$. This model is related to the truncated Schwinger model in the presence of disordered mass or chemical potential [Eq. (A1)]. Note that such onsite disorder breaks the spin-flip symmetry that was present in the clean Hamiltonian. Therefore in the disorder case instead of considering only the symmetric sector, we consider symmetric and antisymmetric blocks together i.e., $\mathcal{D} = (L!)/[(L/2)!]^2$. The additive disorder term changes the structure of the potential function c.f. $\mathcal{V}_{\mathcal{R}}$ [Eq. (8)].

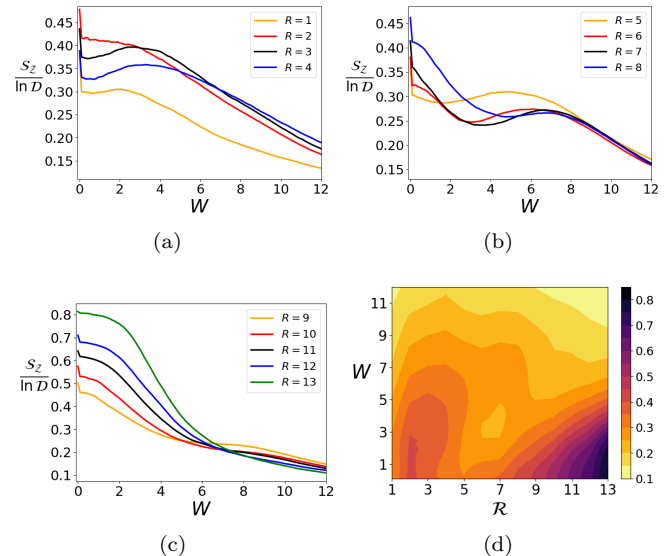


FIG. 7. Participation entropy $\mathcal{S}_{\mathcal{Z}}$ which is averaged over the set \mathcal{Z} and over 150 random realizations of angle φ , as a function of W and \mathcal{R} . $L = 14, U = 1.2$. $\mathcal{D} = 3432$. In the last subfigure (d) we exclude the $W = 0$ cases.

For computational convenience, we choose $L = 14$ and $U = 1.2$ and show the participation entropies \mathcal{S} as a function of disorder strength W for variation of interaction ranges at Fig. 7. The shown plots of \mathcal{S} are averaged over the set \mathcal{Z} [Eq. (5)] and scaled by the logarithm of the Hilbert space dimension $\ln \mathcal{D}$.

Figure 7 reveals that the same anomalous behavior of localization volume observed for the clean system is preserved at weaker disorder for all ranges. Introducing disorder with $W = 0.1$ on the clean system reduces the localization volume or \mathcal{S} for all ranges of interaction. For stronger disorder system comes up with more exotic anomalous behaviors. For $\mathcal{R} \leq 8$ [Fig. 7(a)-(b)] we see an initial increase of localization volume with an increase of W , and a decrease of it upon further increase of W . For such a fragmented system, the disorder induces a transition between different parts of the fragmented Hilbert space, which results in growing correlations between them and the corresponding enhancement of the localization volume. The peaks occur when the disorder induces resonance. The increase of \mathcal{S} is more prominent

for the ranges $\mathcal{R} \in \{1, 3, 4, \dots, 8\}$ when the fragmentation induced localization is observed in Fig. 3. The required W increases for longer \mathcal{R} as the energy required to induce resonance between different fragmented sectors increases. For a very strong disorder system starts to show monotonically decreasing localization volume which is similar to the many-body localization.

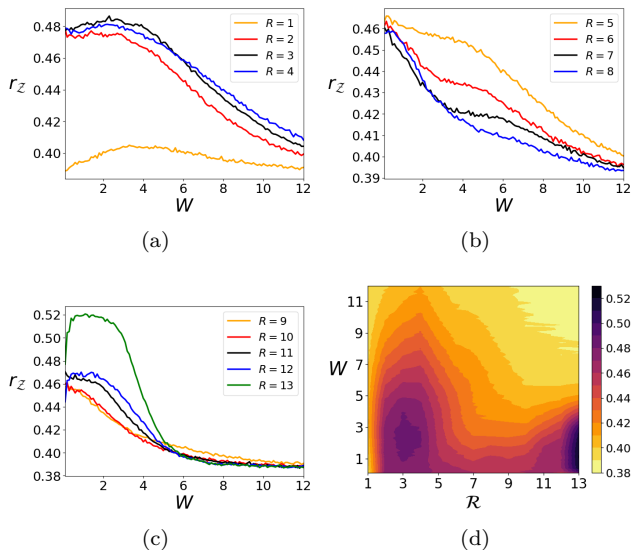


FIG. 8. Spectral gap ratio averaged over the set \mathcal{Z} and over 150 random realizations of angle φ , as a function of W and \mathcal{R} . $L = 14, U = 1.2$. We do not include $W = 0$ case here.

The spectral gap analysis is shown in Fig. 8. For the longest $\mathcal{R} = (L - 1)$, the system is in the ergodic regime for smaller W while for larger W it starts to enter into the nonergodic regime. For all other ranges at some intermediate value of W , we see either an increase of r_Z or a slowdown in the transition from maximum value to minimum. We relate this phenomenon with the disorder-induced local ergodicity or correlation between different fragmented sectors. For very large W the system is near to a many-body localized like regime.

V. CONCLUSION

We have discussed the localization properties of a 1D spin model with interaction strength dependent on the location of interacting spins for different ranges of interactions. Our model captures a lattice Schwinger model with a truncated range of interaction [see Appendix A for details]. The work shows that the localization properties do not change monotonically with the change of interaction range as one could expect naively. We explain this nonmonotonic behavior as a competition between Hilbert space fragmentation and quantum correlations. The effect remains unchanged in the presence of weaker disorder potentials. Our work contributes to the important question of many-body system properties under long-range

interactions which has an increasing physical relevance. It helps us to understand the nature of Coulomb-type interaction as well as the lattice gauge theory models in one dimension. The truncated or finite range of interactions may be associated with the presence of a charge screening or shielding effect. We emphasize that the purpose of this work is not to explore the details of many-body localization transition from ergodic to nonergodic phases, but to report the nonmonotonic behavior of the localization volumes.

In the future, we would like to extend to a higher dimensional lattice where the nature of the interaction could change from linear to logarithmic or in different ways [38]. Introduction of sublattice structure and gauge potential flux can introduce different phenomena that need to be investigated.

It is known that the usual XXZ model is simulable by ultracold Rydberg atoms interacting by van-der-Waals forces [50], where the atom states are mapped to spin up and down states. Tuning the van-der-Waals coefficients for different sets of two Rydberg atoms we could map the inhomogeneous linearly growing ZZ long-range interactions while keeping the hopping term short-ranged [Eq. (1)]. One could use the recently implemented XXZ setups in cold ^7Li atoms in optical lattices [51] where anisotropic ZZ interaction parameters can be set by locally controlling the applied magnetic field. It may also be possible to implement our model using a trapped ion-based digital quantum simulator [52].

ACKNOWLEDGMENTS

The authors acknowledge the financial support from the National Science Centre, Poland (grant 2021/03/Y/ST2/00186) within the QuantERA II Programme, which has received funding from the European Union's Horizon 2020 research and innovation programme under Grant Agreement No 101017733. J. Z. acknowledges also the partial support from the National Science Centre, Poland under grant 2019/35/B/ST2/00034. A. M. thanks Bitan De, Pedro Nicácio Falcão, and Adith Sai Aramthottil for useful discussions.

Appendix A: Similarity of our Hamiltonian with modified Lattice Schwinger model

The lattice Schwinger Hamiltonian for the staggered spinless fermions with the electromagnetic gauge poten-

tial reads [53, 54]

$$\begin{aligned} \mathcal{H}_{\text{sch}} = & -i \sum_{n=0}^{L-2} \left(\psi_n^\dagger e^{i\phi_{n,n+1}} \psi_{n+1} - \psi_{n+1}^\dagger e^{-i\phi_{n,n+1}} \psi_n \right) \\ & + U \sum_{n=-1}^{L-1} \mathcal{E}_{n,n+1}^2 + \sum_{n=0}^{L-1} m_n (-1)^n \psi_n^\dagger \psi_n. \end{aligned} \quad (\text{A1})$$

It controls the dynamics of spinless fermion and anti-fermion fields ψ_n coupled to $U(1)$ gauge boson fields $\phi_{n,n+1}$ which acts as vector potential with the temporal gauge, and $\mathcal{E}_{n,n+1}$ is corresponding electric field and conjugate momentum of $\phi_{n,n+1}$. In the lattice representation fermion fields are located at lattice sites n while the gauge fields are at the links between sites. Let us consider the massless case: $m_n = 0$. The presence and absence of particles (or anti-particles) form two possibilities at each site n , i.e. Hilbert space of dimension two. The dynamical fermionic charge operator is defined as

$$\begin{aligned} \mathcal{F}_n = & \psi_n^\dagger \psi_n - \frac{1}{2} [1 - (-1)^n] \begin{pmatrix} 1 & 0 \\ 0 & 1 \end{pmatrix}, \psi_n^\dagger \psi_n = \begin{pmatrix} 1 & 0 \\ 0 & 0 \end{pmatrix} \\ \implies & \mathcal{F}_{n=\text{even}} = \psi_n^\dagger \psi_n, \mathcal{F}_{n=\text{odd}} = \psi_n \psi_n^\dagger. \end{aligned} \quad (\text{A2})$$

In this notation, the particle can only sit at an even site and it is annihilated by operator ψ , while the anti-particle can sit at the odd site only and it is annihilated by operator ψ^\dagger . In the presence of background static charges q_n the discrete Gauss law reads

$$(\mathcal{E}_{n,n+1} - \mathcal{E}_{n-1,n} - \mathcal{F}_n) |\Psi\rangle = q_n |\Psi\rangle. \quad (\text{A3})$$

where $|\Psi\rangle$ are the only allowed physical states. If we set

$$q_n = -\frac{(-1)^n}{2} \quad (\text{A4})$$

the Gauss law turns

$$\mathcal{E}_{n,n+1} - \mathcal{E}_{n-1,n} = \frac{1}{2} \begin{pmatrix} 1 & 0 \\ 0 & -1 \end{pmatrix} = \sigma_n^z. \quad (\text{A5})$$

Jordan-Wigner transformation [55]

$$\psi_n = \prod_{j=0}^{n-1} [2ie^{-i\phi_{j,j+1}} \sigma_j^z] \sigma_n^- \quad (\text{A6})$$

with Pauli spin matrices: $\sigma_n^+ = \begin{pmatrix} 0 & 1 \\ 0 & 0 \end{pmatrix}$, $\sigma_n^- = \begin{pmatrix} 0 & 0 \\ 1 & 0 \end{pmatrix}$ and σ_n^z turns the hopping part of the Hamiltonian to

$$- \sum_{n=0}^{L-2} (\sigma_n^+ \sigma_{n+1}^- + \sigma_n^- \sigma_{n+1}^+) \quad (\text{A7})$$

which is the XX part of the usual XXZ spin chain model.

For our work, we modify the gauge field energy term of the lattice Schwinger model with link g_n dependent terms

$$U \sum_{n=-1}^{L-1} g_n \mathcal{E}_{n,n+1}^2. \quad (\text{A8})$$

If we choose $\mathcal{E}_{-1,0} = 0$ from Gauss law [Eq. (A5)] we obtain

$$\begin{aligned} \mathcal{E}_{0,1} = \sigma_0^z & \implies \mathcal{E}_{1,2} = \sigma_1^z + \sigma_0^z \\ \implies \dots & \implies \mathcal{E}_{n,n+1} = \sum_{j=0}^n \sigma_j^z. \end{aligned} \quad (\text{A9})$$

Therefore the energy term turns

$$\begin{aligned} U \sum_{n=0}^{L-1} g_n \mathcal{E}_{n,n+1}^2 & = \sum_{n=0}^{L-1} g_n \left(\sum_{j=0}^n \sigma_j^z \right)^2 \\ & = g_0 (\sigma_0^z)^2 + g_1 (\sigma_0^z + \sigma_1^z)^2 \\ & + g_2 (\sigma_0^z + \sigma_1^z + \sigma_2^z)^2 + \dots + g_{L-1} \left(\sum_{j=0}^{L-1} \sigma_j^z \right)^2. \end{aligned} \quad (\text{A10})$$

We use the fact the $(\sigma_j^z)^2$ is proportional to the identity and, hence can be treated as an additional constant and unimportant, therefore upto these additional constants

$$\begin{aligned} U \sum_{n=0}^{L-1} g_n \mathcal{E}_{n,n+1}^2 & = 2\sigma_0^z \sigma_1^z \sum_{j=1}^{L-1} g_j + 2[\sigma_0^z \sigma_2^z + \sigma_1^z \sigma_2^z] \sum_{j=2}^{L-1} g_j \\ & + 2[\sigma_0^z \sigma_3^z + \sigma_1^z \sigma_3^z + \sigma_2^z \sigma_3^z] \sum_{j=3}^{L-1} g_j \\ & + \dots + 2 \left[\sum_{n=0}^{L-2} \sigma_n^z \sigma_{L-1}^z \right] g_{L-1}. \end{aligned} \quad (\text{A11})$$

To produce our model Hamiltonian [Eq. (1)] with longest range of ZZ interaction $\mathcal{R} = L - 1$ we need to set

$$\begin{aligned} \sum_{j=p}^{L-1} g_j & = \frac{p}{2}; \quad p = 1, 2, \dots, L-1 \\ \implies g_1 = g_2 = \dots = g_{L-2} & = -\frac{1}{2}, \quad g_{L-1} = \frac{L-1}{2}. \end{aligned} \quad (\text{A12})$$

This is the gauge energy term in a lattice Schwinger Hamiltonian in the presence of a defect at a boundary. Therefore for the interaction range $\mathcal{R} < (L - 1)$ the Hamiltonian [Eq. (1)] represents a truncated version of the modified Schwinger Hamiltonian.

Appendix B: Plots of S_Z for the extended U

b. $\mathcal{R} = 2$

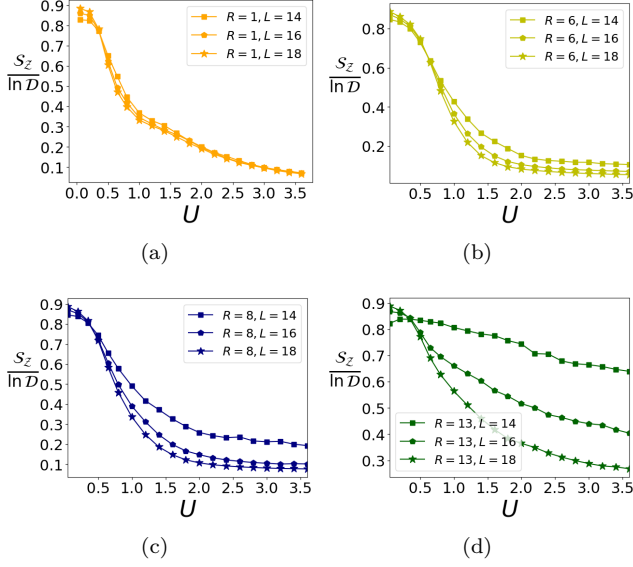


FIG. 9. Plots (a)-(d): $S_Z / \ln \mathcal{D}$ as a function of interaction parameter U for various L and \mathcal{R} for the clean system.

Appendix C: DC field potential part [Eq. (8)] of interacting Hamiltonian for clean system

Here we derive the form of the tilted potential term for general \mathcal{R} after checking the expressions for a few special ranges.

a. $\mathcal{R} = 1$

$$\begin{aligned}
 V_1 &= -\frac{U}{2} \sum_{n=0}^{L-2} (n+1) (\hat{N}_n + \hat{N}_{n+1}) \\
 &= -\frac{U}{2} \hat{N}_0 - \frac{U}{2} (L-1) \hat{N}_{L-1} - \frac{U}{2} \sum_{n=1}^{L-2} (2n+1) \hat{N}_n \\
 &= \frac{UL}{2} \hat{N}_{L-1} - \frac{U}{2} \sum_{n=0}^{L-1} 2n \hat{N}_n - \frac{UL}{4}, \quad (C1)
 \end{aligned}$$

where in the last term we used the total spin zero condition which implies a half-filled lattice $\sum_n \hat{N}_n = L/2$.

$$\begin{aligned}
 V_2 &= V_1 - \frac{U}{2} \sum_{n=0}^{L-3} (n+2) (\hat{N}_n + \hat{N}_{n+2}) \\
 &= -\frac{U}{2} [2\hat{N}_0 + 3\hat{N}_1 + (L-1)\hat{N}_{L-1} + (L-2)\hat{N}_{L-2}] \\
 &\quad - \frac{U}{2} \sum_{n=2}^{L-3} (2n+2) \hat{N}_n + V_1 \\
 &= -\frac{UL}{2} - \frac{U}{2} [\hat{N}_1 + (L-3)\hat{N}_{L-1} + (L-4)\hat{N}_{L-2}] \\
 &\quad - \frac{U}{2} \sum_{n=2}^{L-3} 2n \hat{N}_n + V_1 \\
 &= -\frac{U}{2} [3\hat{N}_1 + (2L-5)\hat{N}_{L-1} + (3L-8)\hat{N}_{L-2}] - \frac{U}{2} \sum_{n=2}^{L-3} 4n \hat{N}_n \\
 &= \frac{U}{2} [\hat{N}_1 + (2L+1)\hat{N}_{L-1} + L\hat{N}_{L-2}] - \frac{U}{2} \sum_{n=0}^{L-1} 4n \hat{N}_n. \quad (C2)
 \end{aligned}$$

In the second from the last line, we omitted the constant terms.

c. $\mathcal{R} = 3$

$$\begin{aligned}
 V_3 &= V_2 - \frac{U}{2} \sum_{n=0}^{L-4} (n+3) (\hat{N}_n + \hat{N}_{n+3}) \\
 &= -\frac{U}{2} \left[3\hat{N}_0 + 4\hat{N}_1 + 5\hat{N}_2 + \sum_{p=1}^3 (L-p) \hat{N}_{L-p} \right] \\
 &\quad - \frac{U}{2} \sum_{n=3}^{L-4} (2n+3) \hat{N}_n + V_2 \\
 &= -\frac{U}{2} \left[\hat{N}_1 + 2\hat{N}_2 + \sum_{p=1}^3 (L-p-3) \hat{N}_{L-p} \right] \\
 &\quad - \frac{U}{2} \sum_{n=3}^{L-4} 2n \hat{N}_n - \frac{3UL}{4} + V_2 \\
 &= -\frac{U}{2} [4\hat{N}_1 + 10\hat{N}_2] - \frac{U}{2} \sum_{n=3}^{L-4} 6n \hat{N}_n \\
 &\quad - \frac{U}{2} [(3L-9)\hat{N}_{L-1} + (4L-13)\hat{N}_{L-2} + (5L-18)\hat{N}_{L-3}] \\
 &= -\frac{U}{2} \sum_{n=0}^{L-1} 6n \hat{N}_n + \frac{U}{2} [2\hat{N}_1 + 2\hat{N}_2 + (3L+3)\hat{N}_{L-1} \\
 &\quad + (2L+1)\hat{N}_{L-2} + L\hat{N}_{L-3}], \quad (C3)
 \end{aligned}$$

where again we omitted the constant term coming from the total magnetization conservation.

Therefore for a general \mathcal{R} the resulting term reads

$$\begin{aligned}
V_{\mathcal{R}} = & -U\mathcal{R} \sum_{n=0}^{L-1} n\hat{N}_n + \frac{U}{2} \sum_{n=0}^{\mathcal{R}-1} n(\mathcal{R}-n)\hat{N}_n \\
& + \frac{U}{4} \sum_{n=0}^{\mathcal{R}} [2nL + n(n-1)] \hat{N}_{L-\mathcal{R}+n-1}. \quad (\text{C4})
\end{aligned}$$

-
- [1] D. A. Abanin, E. Altman, I. Bloch, and M. Serbyn, Colloquium: Many-body localization, thermalization, and entanglement, *Rev. Mod. Phys.* **91**, 021001 (2019).
- [2] V. Oganesyan and D. A. Huse, Localization of interacting fermions at high temperature, *Phys. Rev. B* **75**, 155111 (2007).
- [3] F. Alet and N. Laflorencie, Many-body localization: An introduction and selected topics, *Comptes Rendus Physique* **19**, 498 (2018).
- [4] P. Sierant and J. Zakrzewski, Challenges to observation of many-body localization, *Phys. Rev. B* **105**, 224203 (2022).
- [5] S. Iyer, V. Oganesyan, G. Refael, and D. A. Huse, Many-body localization in a quasiperiodic system, *Phys. Rev. B* **87**, 134202 (2013).
- [6] F. A. An, K. Padavić, E. J. Meier, S. Hegde, S. Ganeshan, J. H. Pixley, S. Vishveshwara, and B. Gadway, Interactions and mobility edges: Observing the generalized aubry-andré model, *Phys. Rev. Lett.* **126**, 040603 (2021).
- [7] K. Huang, D. Vu, S. D. Sarma, and X. Li, Interaction-enhanced many body localization in a generalized aubry-andré model (2023), [arXiv:2305.20090](https://arxiv.org/abs/2305.20090) [cond-mat.dis-nn].
- [8] A. S. Aramthottil, T. Chanda, P. Sierant, and J. Zakrzewski, Finite-size scaling analysis of the many-body localization transition in quasiperiodic spin chains, *Phys. Rev. B* **104**, 214201 (2021).
- [9] E. van Nieuwenburg, Y. Baum, and G. Refael, From bloch oscillations to many-body localization in clean interacting systems, *Proceedings of the National Academy of Sciences* **116**, 9269 (2019).
- [10] M. Schulz, C. A. Hooley, R. Moessner, and F. Pollmann, Stark Many-Body Localization, *Phys. Rev. Lett.* **122**, 040606 (2019).
- [11] S. R. Taylor, M. Schulz, F. Pollmann, and R. Moessner, Experimental probes of stark many-body localization, *Phys. Rev. B* **102**, 054206 (2020).
- [12] Q. Guo, C. Cheng, H. Li, S. Xu, P. Zhang, Z. Wang, C. Song, W. Liu, W. Ren, H. Dong, R. Mondaini, and H. Wang, Stark Many-Body Localization on a Superconducting Quantum Processor, *Phys. Rev. Lett.* **127**, 240502 (2021).
- [13] S. Scherg, T. Kohlert, P. Sala, F. Pollmann, B. H. Madhusudhana, I. Bloch, and M. Aidelsburger, Observing non-ergodicity due to kinetic constraints in tilted Fermi-Hubbard chains, *Nature Communications* **12**, 10.1038/s41467-021-24726-0 (2021).
- [14] E. V. H. Doggen, I. V. Gornyi, and D. G. Polyakov, Stark many-body localization: Evidence for hilbert-space shattering, *Phys. Rev. B* **103**, L100202 (2021).
- [15] R. Yao, T. Chanda, and J. Zakrzewski, Nonergodic dynamics in disorder-free potentials, *Annals of Physics* **435**, 168540 (2021).
- [16] M. Kormos, M. Collura, G. Takács, and P. Calabrese, Real-time confinement following a quantum quench to a non-integrable model, *Nature Physics* **13**, 246 (2016).
- [17] T. Chanda, J. Zakrzewski, M. Lewenstein, and L. Tagliacozzo, Confinement and lack of thermalization after quenches in the bosonic schwinger model, *Phys. Rev. Lett.* **124**, 180602 (2020).
- [18] Z.-C. Yang, F. Liu, A. V. Gorshkov, and T. Iadecola, Hilbert-space fragmentation from strict confinement, *Phys. Rev. Lett.* **124**, 207602 (2020).
- [19] T. Iadecola and M. Žnidarič, Exact localized and ballistic eigenstates in disordered chaotic spin ladders and the Fermi-Hubbard model, *Phys. Rev. Lett.* **123**, 036403 (2019).
- [20] M. Schechter and T. Iadecola, Weak ergodicity breaking and quantum many-body scars in spin-1 XY magnets, *Phys. Rev. Lett.* **123**, 147201 (2019).
- [21] F. M. Surace, P. P. Mazza, G. Giudici, A. Leroose, A. Gambassi, and M. Dalmonte, Lattice Gauge Theories and String Dynamics in Rydberg Atom Quantum Simulators, *Phys. Rev. X* **10**, 021041 (2020).
- [22] G. Magnifico, M. Dalmonte, P. Facchi, S. Pascazio, F. V. Pepe, and E. Ercolessi, Real Time Dynamics and Confinement in the \mathbb{Z}_n Schwinger-Weyl lattice model for 1+1 QED, *Quantum* **4**, 281 (2020).
- [23] U. Gavish and Y. Castin, Matter-wave localization in disordered cold atom lattices, *Phys. Rev. Lett.* **95**, 020401 (2005).
- [24] A. Smith, J. Knolle, D. Kovrizhin, and R. Moessner, Disorder-free localization, *Phys. Rev. Lett.* **118**, 266601 (2017).
- [25] C. Danieli, A. Andreanov, and S. Flach, Many-body flat-band localization, *Phys. Rev. B* **102**, 041116 (2020).
- [26] A. L. Burin, Many-body delocalization in a strongly disordered system with long-range interactions: Finite-size scaling, *Phys. Rev. B* **91**, 094202 (2015).
- [27] A. L. Burin, Localization in a random xy model with long-range interactions: Intermediate case between single-particle and many-body problems, *Phys. Rev. B* **92**, 104428 (2015).
- [28] A. O. Maksymov and A. L. Burin, Many-body localization in spin chains with long-range transverse interactions: Scaling of critical disorder with system size, *Phys. Rev. B* **101**, 024201 (2020).
- [29] W.-H. Li, X. Deng, and L. Santos, Hilbert space shattering and disorder-free localization in polar lattice gases, *Phys. Rev. Lett.* **127**, 260601 (2021).
- [30] A. S. Aramthottil, M. Łacki, L. Santos, and J. Zakrzewski, Role of interaction-induced tunneling in the dynamics of polar lattice bosons, *Phys. Rev. B* **107**, 104305 (2023).
- [31] H. Korbmayer, P. Sierant, W. Li, X. Deng, J. Za-

- krzewski, and L. Santos, Lattice control of nonergodicity in a polar lattice gas, *Phys. Rev. A* **107**, 013301 (2023).
- [32] C. Cheng, Many-body localization in clean chains with long-range interactions, *Phys. Rev. B* **108**, 155113 (2023).
- [33] X.-P. Jiang, R. Qi, S. Yang, Y. Hu, and G. Yang, Stark many-body localization with long-range interactions (2023), [arXiv:2307.12376](https://arxiv.org/abs/2307.12376) [cond-mat.dis-nn].
- [34] S. Baier, M. J. Mark, D. Petter, K. Aikawa, L. Chomaz, Z. Cai, M. Baranov, P. Zoller, and F. Ferlaino, Extended bose-hubbard models with ultracold magnetic atoms, *Science* **352**, 201 (2016).
- [35] L. Su, A. Douglas, M. Szurek, R. Groth, S. F. Ozturk, A. Krahn, A. H. Hébert, G. A. Phelps, S. Ebadi, S. Dickerson, F. Ferlaino, O. Marković, and M. Greiner, Dipolar quantum solids emerging in a hubbard quantum simulator (2023), [arXiv:2306.00888](https://arxiv.org/abs/2306.00888) [cond-mat.quant-gas].
- [36] L. Chomaz, I. Ferrier-Barbut, F. Ferlaino, B. Laburthe-Tolra, B. L. Lev, and T. Pfau, Dipolar physics: a review of experiments with magnetic quantum gases, *Reports on Progress in Physics* **86**, 026401 (2022).
- [37] N. Defenu, T. Donner, T. Macrì, G. Pagano, S. Ruffo, and A. Trombettoni, Long-range interacting quantum systems, *Rev. Mod. Phys.* **95**, 035002 (2023).
- [38] R. M. Nandkishore and S. L. Sondhi, Many-body localization with long-range interactions, *Phys. Rev. X* **7**, 041021 (2017).
- [39] P. Weinberg and M. Bukov, QuSpin: a Python package for dynamics and exact diagonalisation of quantum many body systems part I: spin chains, *SciPost Phys.* **2**, 003 (2017).
- [40] P. Weinberg and M. Bukov, QuSpin: a Python package for dynamics and exact diagonalisation of quantum many body systems. Part II: bosons, fermions and higher spins, *SciPost Phys.* **7**, 020 (2019).
- [41] D.-Z. Wang, H. Zhu, J. Cui, J. Argüello-Luengo, M. Lewenstein, G.-F. Zhang, P. Sierant, and S.-J. Ran, Eigenstate thermalization and its breakdown in quantum spin chains with inhomogeneous interactions (2023), [arXiv:2310.19333](https://arxiv.org/abs/2310.19333) [quant-ph].
- [42] P. Sala, T. Rakovszky, R. Verresen, M. Knap, and F. Pollmann, Ergodicity breaking arising from hilbert space fragmentation in dipole-conserving hamiltonians, *Physical Review X* **10**, 011047 (2020).
- [43] V. Khemani, M. Hermele, and R. Nandkishore, Localization from Hilbert space shattering: From theory to physical realizations, *Phys. Rev. B* **101**, 174204 (2020).
- [44] S. Moudgalya, B. A. Bernevig, and N. Regnault, Quantum many-body scars and hilbert space fragmentation: a review of exact results, *Reports on Progress in Physics* **85**, 086501 (2022).
- [45] N. Macé, F. Alet, and N. Laflorencie, Multifractal scalings across the many-body localization transition, *Phys. Rev. Lett.* **123**, 180601 (2019).
- [46] I. Bengtsson and K. Życzkowski, *Geometry of Quantum States: An Introduction to Quantum Entanglement* (Cambridge University Press, Cambridge UK, 2006).
- [47] D. J. Luitz, N. Laflorencie, and F. Alet, Many-body localization edge in the random-field heisenberg chain, *Phys. Rev. B* **91**, 081103 (2015).
- [48] R. Yao, T. Chanda, and J. Zakrzewski, Many-body localization in tilted and harmonic potentials, *Phys. Rev. B* **104**, 014201 (2021).
- [49] T. Chanda, R. Yao, and J. Zakrzewski, Coexistence of localized and extended phases: Many-body localization in a harmonic trap, *Phys. Rev. Res.* **2**, 032039 (2020).
- [50] R. Ferracini Alves, *Realization of a Heisenberg XXZ spin system using Rydberg atoms*, Ph.D. thesis (2022).
- [51] P. N. Jepsen, J. Amato-Grill, I. Dimitrova, W. W. Ho, E. Demler, and W. Ketterle, Spin transport in a tunable heisenberg model realized with ultracold atoms, *Nature* **588**, 403–407 (2020).
- [52] N. H. Nguyen, M. C. Tran, Y. Zhu, A. M. Green, C. H. Alderete, Z. Davoudi, and N. M. Linke, Digital quantum simulation of the schwinger model and symmetry protection with trapped ions, *PRX Quantum* **3**, 020324 (2022).
- [53] J. Kogut and L. Susskind, Hamiltonian formulation of wilson’s lattice gauge theories, *Phys. Rev. D* **11**, 395 (1975).
- [54] T. Banks, L. Susskind, and J. Kogut, Strong-coupling calculations of lattice gauge theories: (1 + 1)-dimensional exercises, *Phys. Rev. D* **13**, 1043 (1976).
- [55] C. J. Hamer, Z. Weihong, and J. Oitmaa, Series expansions for the massive schwinger model in hamiltonian lattice theory, *Phys. Rev. D* **56**, 55 (1997).